Strong gravitational lensing analysis of the Cosmic Seahorse observation

Claudi Vall Müller
*Facultat de Física, Universitat de Barcelona, Diagonal 645, 08028 Barcelona, Spain.**

Advisor: Jordi Miralda-Escudé

Abstract: Strong gravitational lensing provides a powerful tool for studying the density profiles of dark matter halos in massive galaxy clusters. In this work, we apply a strong lensing analysis to a recent high-resolution JWST observation of a redshift $z = 1.605$ galaxy (WISE J122651.0+214958.8, dubbed Cosmic Seahorse). This galaxy is observed in three different images in the sky, two of which form a highly elongated radial arc near the main galaxy of the foreground galaxy cluster (SDSS J1226+2149). After observing an Einstein radius of $\theta_E = 20.4''$, we obtain a mass-to-light ratio of $\Upsilon \simeq 104\Upsilon_\odot$ for the main galaxy of the foreground cluster, far beyond the expected values for stellar systems. We numerically show that NFW profiles with parametric exponents for the foreground lensing galaxies are able to reproduce the three observed images. The obtained exponents for the main lensing galaxy are $\beta \simeq 0.7$ for the inner region of the mass distribution and $\gamma \simeq 3.4$ for the outer one.

I. INTRODUCTION

One of the direct predictions of the theory of General Relativity is that strong gravitational fields bend light rays around them [1]. This gravitational lensing effect ranges from changing the observed position of stars [2] to making distant galaxies appear larger, distorted, and even multiple times in the sky [3], providing valuable information about both the light source and the foreground lensing mass distribution.

Information about mass distributions is of remarkable importance when considering that $\sim 85\%$ of the mass of the universe is made of dark matter [4], a hypothetical form of collisionless matter that does not interact with light and therefore remains invisible to our telescopes.

On large-scale structures such as galaxies and galaxy clusters, the collisionless dark matter contribution (as opposed to the stellar contribution) dominates the mass density in the outer parts of the structure, and is therefore usually referred to as a dark matter halo. Gravitational lensing provides a powerful tool for studying the properties of dark matter halos, such as their density profiles, which is the main interest of this work. Hints on the nature of dark matter may hide in their density profiles, especially close to the halo centers.

Numerical N-body simulations using the standard ΛCDM cosmological model have suggested a halo density profile with an inner power-law $\rho \sim r^{-1}$, and an outer one $\rho \sim r^{-3}$, known as Navarro-Frenk-White (NFW) [5]. This profile is supported by observations of weak lensing in galaxy clusters [6], but rotation curves have instead suggested constant density cores [7]. This *core-cusp* problem motivates the further study of density profiles near the center of dark matter halos.

This work is focused on a recent publicly available image taken by the James Webb Space Telescope (JWST), in which a strongly lensed galaxy (dubbed Cosmic Seahorse) appears three times in the sky, two of them in the form of a radially elongated arc near the largest galaxy of the foreground galaxy cluster. The particular position of the three images is used to estimate a plausible density profile of the foreground galaxies.

Section II discusses the needed mathematical formalism of gravitational lensing for the work. In Section III, the observation of the radially elongated image is presented, and estimations for the foreground galaxy mass and mass-to-light ratio are computed in Section IV. In Section V, we present a simple lens model for reproducing the multiple images of the Cosmic Seahorse observation.

Throughout this work we use a standard flat ΛCDM cosmological model with $\Omega_m = 0.3$, $\Omega_\Lambda = 0.7$ and $H_0 = 70$ km s^{-1} Mpc^{-1}.

II. GRAVITATIONAL LENSING FORMALISM

The aim of this section is to understand how gravitational lensing theory predicts radially elongated images (radial arcs), such as the Cosmic Seahorse, and how tangentially elongated images (tangential arcs) allow us to estimate the foreground galaxy mass. Throughout this section we will follow [8].

Given a general lensing mass distribution, the relation between the source angular position ($\vec{\beta}$) and the observed images ($\vec{\theta}$), known as the lens equation, under the small-angle approximation is $\vec{\theta} = \vec{\beta} + \vec{\alpha}(\vec{\theta})$, where $\vec{\alpha}(\vec{\theta})$ is the total deflected angle of a light ray generating an image at the angular position $\vec{\theta}$. If the gravitational field is weak and the mass distribution is thin, the total deflected angle is linear and the impact position of a light ray is constant along the lens. General Relativity predicts that, given a surface mass density distribution $\Sigma(\vec{\theta})$, the total deflected

*Electronic address: clvallmu7@alumnes.ub.edu

angle is

$$\vec{\alpha}(\vec{\theta}) = \frac{1}{\pi}\int_{\mathbb{R}^2} d^2\vec{\theta}'\kappa(\vec{\theta}')\frac{\vec{\theta}-\vec{\theta}'}{\|\vec{\theta}-\vec{\theta}'\|^2} \quad \text{with } \kappa(\vec{\theta}) \equiv \frac{\Sigma(\vec{\theta})}{\Sigma_{\text{crit}}}, \tag{1}$$

where $\kappa(\vec{\theta})$ is the dimensionless surface density and $\Sigma_{\text{crit}} \equiv c^2/(4\pi G) \times D_s/(D_l D_{ls})$ is the critical surface density for generating multiple images in the sky. D_s, D_l and D_{ls} are the angular diameter distances of the source, lens, and between lens and source.

Similar to a magnifying glass, gravitational lenses can also converge light rays and therefore increase the observed flux (S) of a distant source. The observable consequence of this converging effect is a proportional increase in the angular size (ω) of the images in the sky, while keeping their surface brightness (I) constant (brightness theorem). The relation between the observed and intrinsic flux of the source is called magnification (μ) and it is related to the lensing parameters as

$$\mu = \frac{dS}{dS_0} = \frac{I d\omega}{I d\omega_0} = \frac{d^2\theta}{d^2\beta} = \frac{1}{\det\mathcal{A}}\ , \tag{2}$$

where $\mathcal{A}_{ij} \equiv \partial\beta_i/\partial\theta_j$ is the Jacobian matrix between source and image position and can be written as

$$\mathcal{A} = \begin{pmatrix} 1-\kappa(\vec{\theta})-\gamma_1(\vec{\theta}) & -\gamma_2(\vec{\theta}) \\ -\gamma_2(\vec{\theta}) & 1-\kappa(\vec{\theta})+\gamma_1(\vec{\theta}) \end{pmatrix}, \tag{3}$$

if $\gamma_1 \equiv (\partial\alpha_1/\partial\theta_1 - \partial\alpha_2/\partial\theta_2)/2$ and $\gamma_2 \equiv \partial\alpha_1/\partial\theta_2$. The magnification of an image as a function of the lens profile will then be

$$\mu(\vec{\theta}) = \frac{1}{(1-\kappa(\vec{\theta}))^2 - \gamma_1(\vec{\theta})^2 - \gamma_2(\vec{\theta})^2}\ . \tag{4}$$

An interesting consequence is that most lens models predict positions where $\det\mathcal{A} = 0$ and therefore where the magnification formally diverges. This unphysical result corresponds to the convergence of several light rays to a single point. Even though there are realistic phenomena such as the finite size of the source limiting this magnification, positions where $\det\mathcal{A} = 0$, called critical curves, still predict high magnification areas and are therefore of huge importance. The source positions of images lying on the critical curves are called caustics. Our cases of interest, radial and tangential arcs, are both examples of images lying close to the critical curves of the lens model. Gravitational lensing theory allows us to numerically compute the position of the critical curves and caustics given a known lens model.

It is now interesting to apply the above reasoning to a generic polar symmetric mass distribution, i.e., $\kappa(\vec{\theta}) = \kappa(\theta)$. One can show that, in this case, the Jacobian reads $\det\mathcal{A} = (1-\bar{\kappa})(1+\bar{\kappa}-2\kappa)$, where $\bar{\kappa}(\theta)$ is the enclosed mean dimensionless surface density within radius θ. From here it follows that the predicted critical curves are $\bar{\kappa}(\theta) = 1$ and $\bar{\kappa}(\theta) = 2\kappa(\theta) - 1$. Because the direction of image elongation (given by the Jacobian matrix eigenvector of the vanishing eigenvalue) is in the first case tangential and radial in the second, the former are called tangential critical curves and the latter radial ones.

If a source happens to lie on the tangential caustic, it will form a circular image on the tangential critical curve known as an Einstein ring, with a radius called Einstein radius (θ_E). From the above condition of tangential critical curves, it follows that the enclosed mass within θ_E is

$$M = \pi\theta_E^2 D_l^2 \times \Sigma_{\text{crit}}\ . \tag{5}$$

This result allows us to estimate the mass of the main foreground galaxy in the Cosmic Seahorse observation in Section IV.

An important example of mass distribution with polar symmetry is the NFW profile, which has the form $\rho(r) = \rho_0/[(r/R_s)(1+r/R_s)^2]$. As shown in Figure 1 this distribution can reproduce both radial and tangential arcs. As previously mentioned, this NFW profile is supported by dark matter simulations and observations, and will therefore be the studied model for the Cosmic Seahorse observation.

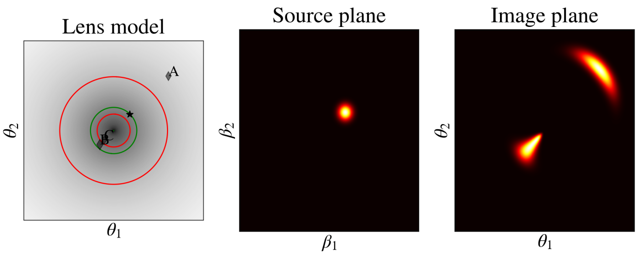

FIG. 1: Left: dimensionless surface density (κ) plot for a NFW mass distribution, with the corresponding caustics (green) and critical curves (red). A source lying on the star marker produces images A, B and C. Center: intrinsic surface brightness plot (arbitrary units) of a circular source. Right: lensed (observed) surface brightness plot generated by the circular source. We can clearly identify a tangential (upper right) and a radial (lower left) arc.

III. COSMIC SEAHORSE OBSERVATION

The main focus of the work is the study of a recent JWST observation [15] of a redshift $z_S = 1.605$ lensed galaxy (WISE J122651.0+214958.8, dubbed Cosmic Seahorse) by the redshift $z_L = 0.435$ foreground cluster SDSS J1226+2149 [9]. The position of the main galaxy of the foreground cluster in equatorial coordinates is $(\alpha, \delta) = (12^{\text{hr}}\,26^{\text{m}}\,51.151^{\text{s}}, +21°49'52''.15)$. The observed cluster is shown in Figure 2, and we can clearly identify the lower redshift (bluer) foreground galaxies from the lensing cluster and the higher redshift (redder) lensed sources from the background. The Cosmic Seahorse red galaxy appears in three different images, two of which constitute a radial arc near the main galaxy of the foreground lensing cluster.

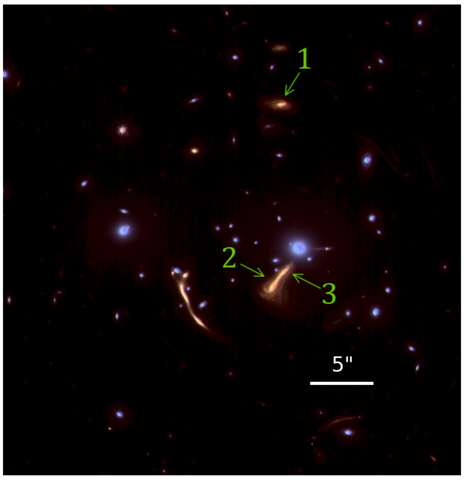

FIG. 2: Composite image of the central area of the J1226+2149 galaxy cluster, using the F444W, F356W and F277W NIRCam filters as RGB colors. The three multiple images from the Cosmic Seahorse galaxy are marked with green indicators.

IV. MAIN FOREGROUND GALAXY'S MASS COMPUTATION

As discussed in Section II, the observation of a tangential critical curve allows us to compute the enclosed mass of a polar symmetric mass distribution within the Einstein radius (θ_E) of the critical curve. Even if tangential arcs appear on critical curves only if the source lies exactly on the caustic, high tangentially magnified images are close to the critical curve and can be used as indicators of it.

This is the case of the above presented observation. In the previous Figure 2, we can identify a background red galaxy that has been strongly tangentially lensed on the left side of the Cosmic Seahorse radial arc. We use this image to estimate the Einstein radius of the mass distribution, assuming polar symmetry for the foreground galaxy and that its center coincides with the center of light. The Einstein radius computation is shown in Figure 3 and the obtained value is $\theta_E \simeq 20.4''$. Knowing both source and lens redshifts and therefore their angular diameter distances, we use equation (5) to estimate the enclosed mass within θ_E. The obtained value is $M_{\text{enclosed}} \simeq 9.4 \times 10^{13} M_\odot$, which is reasonable when compared to other existing estimations [10].

It is interesting now to compare the obtained mass with the total luminosity of the foreground galaxy. It is common to define the mass-to-light ratio parameter, by taking the ratio between the mass of a spatial volume and its luminosity. Stellar systems composed entirely of stars have typical values for the mass-to-light ratio of

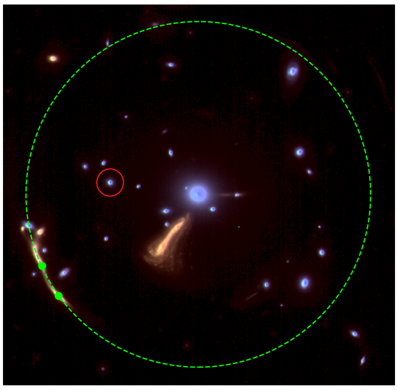

FIG. 3: Tangential critical curve estimation (green dotted line) from the observation of two tangentially magnified images (green dots). The obtained Einstein radius is $\theta_E = 20.4''$. The red circle marks the studied galaxy for the total luminosity estimation.

$\Upsilon \equiv M/L \sim 1$–$10\Upsilon_\odot$ [11], where $\Upsilon_\odot$ is the solar mass-to-light ratio. However, volumes with a high dark matter contribution may have mass-to-light ratios up to $\Upsilon \sim 500\Upsilon_\odot$.

The luminosity estimation can be derived from the publicly available apparent magnitude (m) of the main foreground galaxy of $m_r = 17.70$ [12]. Because the light we detect is a factor $(1+z_L)$ redder than the emitted, we decide to compare the red filter (658 nm) for the source with the green one (464 nm) for the solar absolute magnitude ($\mathcal{M}$) of $\mathcal{M}_\odot = 4.68$ [13]. From the absolute magnitude definition, the luminosity of the foreground galaxy can be computed as $L/L_\odot = 100^{(\mathcal{M}_\odot - \mathcal{M})/5}$, where $\mathcal{M} = m - 5\log_{10}(D_L/1\text{ pc}) + 5$ and $D_L = (1+z)^2 D_l$ is the luminosity distance of the foreground galaxy. The obtained value for the luminosity of this main foreground galaxy is $L = 3.6 \times 10^{11} L_\odot$.

To make a fair comparison with the above computed mass, we should take into account the rest of the luminosity enclosed in θ_E other than the main galaxy. We estimate this contribution by taking the galaxy marked with a red circle in Figure 3 as a representative of all ~ 22 smaller galaxies observed. From the publicly available data (F444W filter), we compute a flux ratio between the 22 smaller galaxies and the main one of ~ 1.5. With a total luminosity within θ_E of $\sim 2.5L$, we obtain a mass-to-light ratio of $\Upsilon \simeq 104\Upsilon_\odot$, far beyond the range of stellar systems. This value for the mass-to-light ratio provides a reasonable hint that the total mass of the system is dominated by non-light-emitting matter, with collisionless dark matter as the main candidate.

V. NUMERICAL LENS MODELS

In this section we present the methods and results of finding a plausible lens model (foreground mass distribution) for reproducing the three main Cosmic Seahorse images. We use the publicly available `Lenstronomy` python package [14], an open-source package for gravitational lens modeling. The features of interest for the work are the image plane construction (lensed images) from a given lens and source models (Figure 1) and the numerical lens equation solver for a given lens model.

The followed methodology consists of optimizing a function that compares observations to the predictions of a given lens and source models. With the goal of testing the robustness of the results, we adopt two different techniques to define this optimizing function, which we call source plane (I) and image plane (II) optimization.

Both optimizing algorithms are applied to a lens model consisting of two generalized NFW profiles for the two main galaxies of the foreground cluster. Each profile assumes NFW profiles with parametric inner (β) and outer (γ) exponents. Each profile reads $\rho(r) = \rho_0/r^\beta \times R_s^\gamma/(r^2 + R_s^2)^{(\gamma-\beta)/2}$ and the standard NFW profile is recovered if $\beta = 1$ and $\gamma = 3$. In case of favoring the existance of a core in the center of the profile, we expect to find $\beta \simeq 0$. The algorithm takes as optimizing parameters the density proportionality constants ($\rho_0^{(1)}$, $\rho_0^{(2)}$), their characteristic radial sizes ($R_s^{(1)}$, $R_s^{(2)}$), and their inner and outer exponents ($\beta^{(1)}$, $\beta^{(2)}$, $\gamma^{(1)}$ and $\gamma^{(2)}$).

Source plane optimization consists in, given a known set of multiple images of the same source, finding their corresponding source positions in a two-dimensional grid and maximizing the overlap between them. A perfect lens model would predict that, when solving the lens equation for each image position, all source positions coincide. In Figure 4 we show a set of selected image pairs, the images of each we assume to correspond to the same source. The criterion for selecting these images is merely observational, and an improved spectroscopic analysis would be performed if the required data were available.

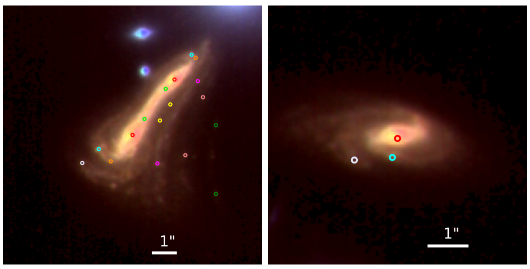

FIG. 4: Set of image pairs marked on the composite RGB image, showing the three images of the Cosmic Seahorse galaxy. All images with circular markers of the same colors are assumed to be multiple images of the same source.

Having computed the total overlap, we run a Nelder-Mead algorithm to repeat the process until an optimal set of parameters for the lens model is found. The best lens model we have found using this method is shown in Figure 5.

We can see that this optimal lens model reproduces all three images (predicted image plane) of the Cosmic Seahorse observation. For these results, we have only used the information of two image pairs (red and cyan) from Figure 4. Adding more image pairs complicates the reproduction of the Cosmic Seahorse's top image. The obtained optimal parameters of interest for the main foreground galaxy (right one of the lens model) are $\rho^{(1)} \simeq 3 \times 10^{16} M_\odot/\mathrm{Mpc}^3$, $R_s^{(1)} \simeq 0.06$ Mpc, and exponents $\beta^{(1)} \simeq 0.7$ and $\gamma^{(1)} = 3.4$. The optimal lens model is similar to a standard NFW model with a central cusp at the origin.

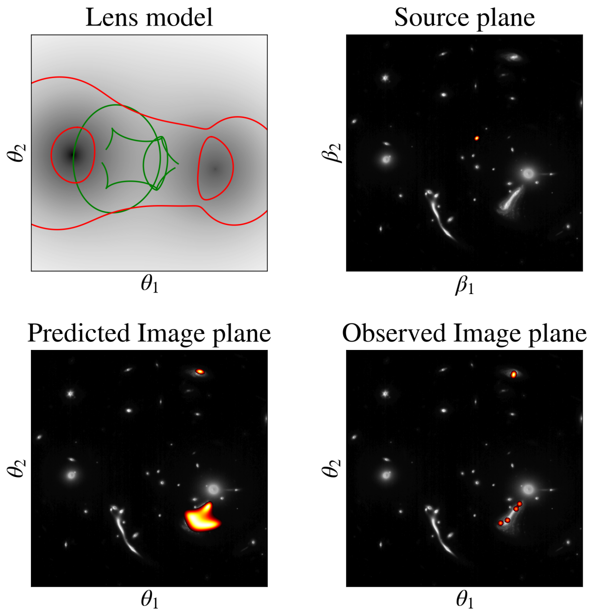

FIG. 5: Optimal lens model configuration for the source plane optimization method. The background black and white image is just a reference indicator. Upper left: dimensionless surface density (κ) plot for the optimal lens model, with its critical curves (red) and caustics (green). This model allows us to construct the source positions (upper right) from the observed images (lower right) and compare them with the predicted ones (lower left) from the source and lens models.

On the other hand, image plane optimization consists in, given a lens and a source model, generating the predicted image plane and then computing the differences to the observed one. A perfect lens model would exactly reproduce the observed image plane.

We take the whole set of images from Figure 4 to construct the observed image plane. For the predicted image plane construction, we generate one single light source, whose position and size are three additional parameters to optimize. By not generating one source for each observed image pair, we lose information about which images are multiple of the same source. Adding this information complicates again the reproduction of the top Cosmic Seahorse image.

We again run a Nelder-Mead algorithm to find the optimal lens model for reproducing the observed image plane. The optimal lens model configuration, with its image plane comparison between prediction and observation, is shown in Figure 6.

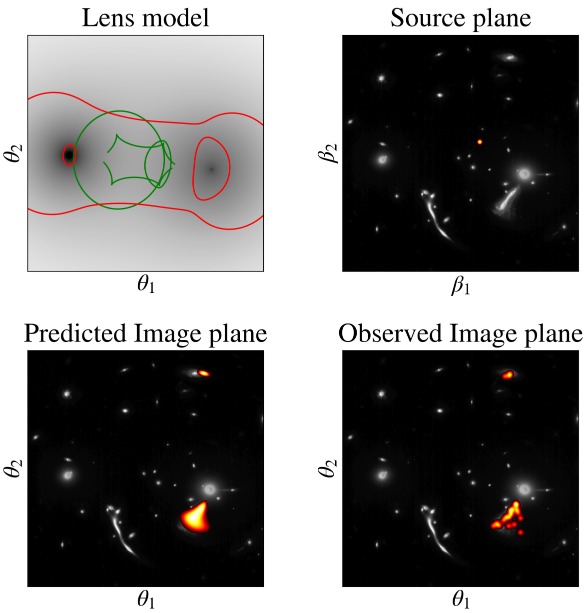

FIG. 6: Optimal lens model configuration for the image plane optimization method. This optimal lens model (upper left) allows us to construct the predicted image plane (lower left) from an optimized source position (upper right) and compare it with the observed image plane (lower right).

The optimal parameters for the main foreground galaxy are $\rho^{(1)} \simeq 1 \times 10^{16} M_{\odot}/\mathrm{Mpc}^3$, $R_s^{(1)} \simeq 0.11$ Mpc, and exponents $\beta^{(1)} \simeq 1.0$ and $\gamma^{(1)} = 3.9$. Again, the results are compatible with a standard NFW profile.

VI. CONCLUSIONS

The distribution of matter in lensing clusters may contain information about the nature and interaction properties of dark matter. In this work, we have used a recent strong lensing observation of a radial arc to estimate the density profile of the main galaxy of the foreground lensing cluster.

From an observed tangential arc, we have obtained a mass-to-light ratio for this foreground galaxy of $\Upsilon \simeq 104\Upsilon_{\odot}$. This high value indicates, as expected, that the total mass is dominated by matter that does not contribute to the galaxy's luminosity, with collisionless dark matter as the main candidate.

We have then numerically constructed lens models using the publicly available Lenstronomy package for reproducing the observed multiple images and the radial arc of a background galaxy. Using two different optimization methodologies, we can reproduce the three images of the lensed galaxy by assuming two spherical foreground distributions with generalized NFW profiles. The results obtained are consistent with standard NFW profiles.

Acknowledgments

I would like to thank my supervisor, Jordi, for his guidance throughout the work. I am grateful to my parents, for their support and curiosity; to Miquel, for his constant support and example; to Andreu, for his interesting thoughts and comments, and to Helena, for her unconditional encouragement and nutritive advice.

[1] A. Einstein, Science **84**, 506 (1936).
[2] F. W. Dyson, A. S. Eddington, and C. Davidson, Philosophical Transactions of the Royal Society of London Series A **220**, 291 (1920).
[3] D. Walsh, R. F. Carswell, and R. J. Weymann, Nature (London) **279**, 381 (1979).
[4] Planck Collaboration, P. A. R. Ade, N. Aghanim, M. Arnaud, M. Ashdown, J. Aumont, C. Baccigalupi, A. J. Banday, R. B. Barreiro, J. G. Bartlett, et al., **594**, A13 (2016), 1502.01589.
[5] J. F. Navarro, C. S. Frenk, and S. D. M. White, Astrophys. J. **462**, 563 (1996), astro-ph/9508025.
[6] N. Okabe, G. P. Smith, K. Umetsu, M. Takada, and T. Futamase, **769**, L35 (2013), 1302.2728.
[7] K. Oman, J. Navarro, A. Fattahi, C. Frenk, T. Sawala, S. White, R. Bower, R. Crain, M. Furlong, M. Schaller, et al., Monthly Notices of the Royal Astronomical Society **452** (2015).
[8] P. Schneider, J. Ehlers, and E. E. Falco, *Gravitational Lenses* (1992).
[9] N. Sulzenauer, H. Dannerbauer, A. Díaz-Sánchez, B. Ziegler, S. Iglesias-Groth, and R. Rebolo, **923**, L27 (2021), 2110.05537.
[10] M. Oguri, M. B. Bayliss, H. Dahle, K. Sharon, M. D. Gladders, P. Natarajan, J. F. Hennawi, and B. P. Koester, **420**, 3213 (2012), 1109.2594.
[11] J. Binney and S. Tremaine, *Galactic dynamics* (1987).
[12] J. Kollmeier, S. F. Anderson, G. A. Blanc, M. R. Blanton, K. R. Covey, J. Crane, N. Drory, P. M. Frinchaboy, C. S. Froning, J. A. Johnson, et al., in *Bulletin of the American Astronomical Society* (2019), vol. 51, p. 274.
[13] K. Čotar, T. Zwitter, G. Traven, J. Kos, M. Asplund, J. Bland-Hawthorn, S. Buder, V. D'Orazi, G. M. de Silva, J. Lin, et al., **487**, 2474 (2019), 1904.04841.
[14] S. Birrer and A. Amara, *Lenstronomy: Multi-purpose gravitational lens modeling software package*, Astrophysics Source Code Library, record ascl:1804.012 (2018).
[15] The data of the observation used in this paper can be found in MAST: `https://doi.org/10.17909/ney1-5w90`.